ISSN: 1004-499X Vol. 37 No. 1 (2025)

# MHD Boundary layer Flow of Hybrid Nanofluids over a Porous Stretching Sheet with Thermal Radiation: A Three-Dimensional Perspective

Yugansha Kabra $a^*$ , Dr. Vivek K. Sharma $^b$ 

PhD Scholar<sup>a\*</sup>, Department of Engineering and Technology (Mathematics), Jagannath University, Sitapura Campus, Jaipur (Rajasthan),

Professor<sup>b</sup>, Faculty of Engineering and Technology, Jagannath University, Sitapura Campus, Jaipur (Rajasthan),

Email: yuganshakabra@gmail.com

**Abstract:** This paper presents a three-dimensional analysis of magnetohydrodynamic (MHD) hybrid nanofluid (HNF) flow over a porous stretching sheet, with the combined effects of thermal radiation and magnetic fields on heat and mass transfer. Using similarity transformations and the Finite Element Method (FEM), the governing equations of momentum, energy, and mass transfer are reformulated and numerically solved. Results demonstrate that increasing the magnetic field parameter (M) from 0.0 to 6.0 leads to a significant thickening of the thermal boundary layer and reduces fluid velocity due to enhanced Lorentz force damping. The temperature profile exhibits slower decay for higher thermal radiation (n = 0.5), indicating efficient radiative heat retention, while higher heat source parameters (q = 0.5) accelerate thermal dissipation. Similarly, increasing the Schmidt number (Sc = 1.0) leads to thinner mass boundary layers due to lower diffusivity, while lower Prandtl numbers (Pr = 1) yield thicker thermal layers compared to higher values (Pr = 7). A comparison with 2023 results shows enhanced accuracy in Sherwood number (Shx) predictions for mass transfer, such as Shx = 1.74370 for M = 0.0 in this study versus 1.74389 in prior literature. These findings underscore the complex interplay between MHD effects, radiation, and porous media and demonstrate the FEM's efficacy in simulating hybrid nanofluid behavior in thermal management system.

**Keywords:** magnetohydrodynamics, hybrid nanofluid, porous stretching sheet, thermal radiation, heat transfer, mass transfer, numerical analysis, Finite Element Method

#### Introduction

Understanding mass and heat transfer processes, particularly mass and heat convection, is crucial for numerous industrial and engineering applications such as cooling devices, chemical reactors, and energy systems. Convective heat transfer is generally classified into natural (or free) convection, caused by buoyancy forces acting on a density difference, and forced convection, when an external force moves the fluid—often resulting in a higher rate of heat transfer [5]. Forced convection, especially where high heat transfer rates are desired, is a popular mechanism for many engineering applications. Forced convection is used in many industrial applications, such as electronics, turbines, and internal combustion engines. As an example, this principle is widely used for the conservation of automotive cooling systems through forced convection, which helps to remove the heat from engine parts in no time and maintains operational efficiency and longevity. In forced convection, external forces, like pumps or fans, are employed to control and amplify the fluid flow, thus making it very efficient for temperature control. As one moves to high-temperature processes and applications such as nuclear reactors, hightemperature plasmas, and power-conversion systems, radiation effects become more important. In such environments, thermal radiation, or the heat-induced emission of electromagnetic waves from a body, is one of the fundamental processes of heat transmission. Radiative heat transfer becomes a significant factor in systems that accurately control temperature, particularly in the aerospace and metallurgical industries. It allows heat to escape regardless of the medium, which, in cases such as low conducting fluids and vacuum, could be the only means of reducing heat, thanks to thermal radiation [10]. Recently, there has been a lot of attention in the combined impacts of thermal radiation, convection, and conduction on flow and heat transfer. Thermal radiation and convection interact and can significantly impact boundary layer behavior, influencing temperature profiles, flow stability, and heat transfer performance. More specifically, these effects are crucial in magnetohydrodynamic

ISSN: 1004-499X Vol. 37 No. 1 (2025)

(MHD) flows, The mechanism of heat transmission and fluid movement becomes more difficult when MHD flows mix a fluid with a magnetic field. MHD is the branch of physics and engineering that deals with the magnetic behavior of people's fluids, which can conduct electricity, specifically plasmas, liquid metals, and saltwater. MHD flows have attracted a lot of interest in applications requiring fluid flow and temperature distribution control. Take, for instance, metallurgical practices, where magnetic fields shape the movement of molten, conductive metals in such a liquid state that they fly to the desired location and pool together. Likewise, in nuclear fusion reactors, MHD helps deal with the plasma flow, which allows successfully running the plant to stable and efficiently extract the generated heat. In MHD flows, a magnetic field gives rise to complex interactions between the flow and the field as a result of the forces enhancing or opposing fluid motion, which changes the temperature and velocity profiles in the boundary layer. MHD flows have been investigated in several fluid flow problems, such as flows along stretching and shrinking sheets. Similar shrinking models are relevant for processes where the plate is getting smaller and must be addressed in processes such as cooling polymer sheets or other external fields. Stretching sheets are typically applied to the polymer sheets' stretching, drawing, and extrusion process. Since flow over a stretching or contracting sheet is crucial to fluid mechanics and heat transmission, it falls within the boundary layers flow category. Because of gravity and thermal factors, the fluid layer next to the surface in these investigations is known as the boundary layer, and it behaves distinctively from the other fluid. The motion of fluid in this region is essential for maximizing heat transfer and mass transfer rates, as well as fluids' stability and surface properties [1].

Apart from these, many researchers have conducted their studies on MHD flows over-stretching sheets, where the magnetic fields and radiation effects were found to affect the thermal and the boundary layer's velocity characteristics. For instance, Hossain and Takhar used the Rosseland diffusion approximation, which is appropriate for optically thick fluids, to study the radiation impacts. In order to comprehend how radiation affects regulating heat transfer rates, they have investigated how radiation affects the boundary-layer motion of a viscous fluid across a semi-infinite heated vertical plate. Building on this work, Shateyi et al. investigate how buoyancy and thermal radiation affect heat and mass transmission across a semi-infinite extending surface with suction and blowing [17]. Their research demonstrated that thermal radiation could regulate the thickness of the thermal boundary layer and, consequently, the rate of heat transfer. Stretching sheets' effects on convective heat transfer have also been evaluated in MHD flow. Samad and Rahman have investigated the impact of thermal radiation on the border layer for unstable MHD flow over a porous vertical plate and discovered that the radiation can significantly change the temperature and velocity fields when a magnetic field is present. Likewise, Samad and Karim studied thermal radiation effects in MHD-free convection flow and the regulation of the temperature field along a flat plate considering a time-dependent suction. Fluid dynamics in porous media is an area of focus related to many practical applications like filtration, oil recovery, and chemical processing. Moreover, the presence of porous media adds resistance to the flow of the fluid, which changes the velocity and temperature profiles and, consequently, the heat transfer rates. MHD flows over porous stretching or shrinking sheets represent an extraordinary challenge to a researcher because they reflect the complication of magnetic forces, thermal radiation, and flow resistance resistive effect due to porosity [8]. This time, we consider these studies by exploring hydro nanofluids' Heat transfer via MHD boundary layer over a permeable shrinking sheet enhanced by thermal radiation. Abstract—Hydro nano fluids comprise fluids with suspended nano-scale particles and are found to have higher thermal conductivity when compared to conventional fluids; thus, they are excellent candidates for heat transfer applications. Hydro nanofluids add one more aspect to the investigation since the heat transfer properties of the nanoparticles influence the heat transfer characteristics of the fluid as a whole. It is important to note that our objective is making a significant effort to explain how hydro nano fluids behave, as when a magnetic field and thermal radiation are incorporated in the boundary layer, we can optimize the parameters that determine temperature, velocity, and concentration. The study's mathematical formulation is accomplished by obtaining dimensionless equations for temperature, concentration, and flow inside the boundary layer [2]. The governing PDEs are reduced through similarity transformations into a system of ODEs, which are solved through numerical methods. Among the primary parameters are the radiation parameter, Schmidt number, Prandtl number, magnetic field parameter, and heat source parameter, and so forth. These parameters are changed so that the boundary layer profiles can be investigated. These findings will help design high-temperature heat transfer systems, where

ISSN: 1004-499X Vol. 37 No. 1 (2025)

accurate control over fluid behavior is essential. These results may benefit the design of electronic cooling systems, improved energy efficiency for heat exchangers, and process optimization in chemical engineering and metallurgical industries. In addition, the findings could have implications for employing magnetic fields and thermal radiation to manipulate the boundary layer properties in hybridnanofluid flows, opening avenues for novel thermal management and fluid control systems. So, to summarize the main idea, this investigation is about the MHD boundary layer flow of hydridnanofluids over a porous shrinking sheet in the presence of thermal radiation. This study attempts to fill this gap between theory and practice for a hybridnanofluid flow analyzed in the presence of magnetic field, thermal radiation, and porosity, essential in advanced heat transfer systems. Optimized cooling in high-temperature electronics is necessary for an efficient Energy Infrastructure, and the insights from this study will assist in developing even more effective heat extraction techniques and enrich the broader fluid mechanics and heat transfer disciplines [11].

#### **Mathematical Formulation:**

Consider an incompressible, steady, three-dimensional water-based hybrid nanofuid flowing above a porous stretchable sheet. A cartesian coordinate system x, y, z - is considered to discuss the problem physically. The x-axis is taken in the horizontal direction, the z-axis is upward and the y-axis is perpendicular to both other axes. The nanofuid is rotating at a constant speed with  $\omega *$  along the z-axis, chemical reaction and, thermal radiation are considered. The flow is induced by a stretching sheet with speeds  $U_w = ax$  and  $V_w = by$  in the x-direction and the y-direction (see Fig. 1). Nanofluid and hybrid nanofluid are considered for this comparative study. The governing equation along with these considerations takes the following form

Governing Equations of the flow, energy and mass transfer are mention below:

#### 1. Continuity Equation:

$$\frac{\partial \mathbf{u}}{\partial \mathbf{x}} + \frac{\partial \mathbf{v}}{\partial \mathbf{y}} + \frac{\partial \mathbf{w}}{\partial \mathbf{z}} = \mathbf{0} \tag{1}$$

- o the velocity components in the directions of x y and z, respectively.
- This equation represents the incompressibility condition in fluid dynamics.

#### 2. Momentum Equations:

$$u\frac{\partial u}{\partial x} + v\frac{\partial u}{\partial y} + w\frac{\partial u}{\partial z} - 2\acute{\omega}v = \frac{\mu_{hnf}}{\rho_{hnf}} \left(\frac{\partial^2 u}{\partial x^2} + \frac{\partial^2 u}{\partial y^2} + \frac{\partial^2 u}{\partial z^2}\right) - \frac{\sigma_{hnf}B_0^2}{\rho_{hnf}}u + \frac{g(\rho\beta_{t})_{hnf}}{\rho_{hnf}}(T - T_{\infty}) + \frac{g(\rho\beta_{c})_{hnf}}{\rho_{hnf}}(C - C_{\infty}) - \frac{\mu_{hnf}u}{\rho_{hnf}K_0}$$
(2)

$$u\frac{\partial v}{\partial x} + v\frac{\partial v}{\partial y} + w\frac{\partial v}{\partial z} + 2\dot{\omega}u = \frac{\mu_{hnf}}{\rho_{hnf}} \left(\frac{\partial^2 v}{\partial x^2} + \frac{\partial^2 v}{\partial y^2} + \frac{\partial^2 v}{\partial z^2}\right) - \frac{\sigma_{hnf}B_0^2}{\rho_{hnf}}v + \frac{g(\rho\beta \ t)_{hnf}}{\rho_{hnf}}(T - T_{\infty}) + \frac{g(\rho\beta^*c)_{hnf}}{\rho_{hnf}}(C - C_{\infty}) - \frac{\mu_{hnf}v}{\rho_{hnf}K_0}v + \frac{g(\rho\beta \ t)_{hnf}}{\rho_{hnf}}(C - C_{\infty}) - \frac{\mu_{hnf}v}{\rho_{hnf}K_0}v + \frac{g(\rho\beta \ t)_{hnf}}{\rho_{hnf}K_0}v + \frac{g(\rho\beta \$$

This equation describes the balance of forces acting in the x-direction and y-direction including viscous, magnetic, buoyancy, and porous medium resistance forces.

## 1. Energy Equation:

$$\begin{split} u\frac{\partial T}{\partial x} + v\frac{\partial T}{\partial y} + w\frac{\partial T}{\partial z} &= \alpha_{hnf} \left(\frac{\partial^2 T}{\partial x^2} + \frac{\partial^2 T}{\partial y^2} + \frac{\partial^2 T}{\partial z^2}\right) + \frac{\sigma_{hnf}B_0^2}{\left(\rho c_p\right)_{hnf}} \left(u^2 + v^2\right) - \frac{1}{\left(\rho c_p\right)_{hnf}} \frac{\partial q_r}{\partial z} + \frac{\mu_{hnf}}{\left(\rho c_p\right)_{hnf}} \left[\left(\frac{\partial u}{\partial z}\right)^2 + \left(\frac{\partial v}{\partial z}\right)^2\right] \\ &+ \frac{\partial T}{\partial y} \cdot \frac{\partial C}{\partial y} + \frac{\partial T}{\partial z} \cdot \frac{\partial C}{\partial z}\right) \right\} + \frac{D_T}{D_\infty} \left(\left(\frac{\partial T}{\partial x}\right)^2 + \left(\frac{\partial T}{\partial y}\right)^2 + \left(\frac{\partial T}{\partial z}\right)^2\right) + \frac{Q_0 (T - T_\infty)}{\left(\rho c_p\right)_{hnf}} \end{split} \tag{4}$$

This equation represents the energy balance, considering convection, thermal conduction, and magnetic heating.

## 2. Concentration Equation:

$$u\frac{\partial C}{\partial x} + v\frac{\partial C}{\partial y} + w\frac{\partial C}{\partial z} = D_B \left(\frac{\partial^2 C}{\partial x^2} + \frac{\partial^2 C}{\partial y^2} + \frac{\partial^2 C}{\partial z^2}\right) + \frac{D_T}{D_\infty} \left(\frac{\partial^2 T}{\partial x^2} + \frac{\partial^2 T}{\partial y^2} + \frac{\partial^2 T}{\partial z^2}\right) - \frac{k_C(C - C_\infty)}{(\rho c_p)_{hnf}}$$
(5)

ISSN: 1004-499X Vol. 37 No. 1 (2025)

This equation governs the concentration distribution of nanoparticles in the fluid, considering

$$\frac{\partial q_r}{\partial z} = -\frac{16\sigma T_{\infty}^3}{3k_1} \frac{\partial^2 T}{\partial z^2}$$
 (6)

$$\begin{split} u\frac{\partial T}{\partial x} + v\frac{\partial T}{\partial y} + w\frac{\partial T}{\partial z} &= \alpha_{hnf} \left(\frac{\partial^2 T}{\partial x^2} + \frac{\partial^2 T}{\partial y^2} + \frac{\partial^2 T}{\partial z^2}\right) + \frac{\sigma_{hnf}B_0^2}{(\rho c_p)_{hnf}} (u^2 + v^2) - \frac{1}{(\rho c_p)_{hnf}} - \frac{16\sigma T_\infty^3}{3k_1} \frac{\partial^2 T}{\partial z^2} + \frac{\mu_{hnf}}{(\rho c_p)_{hnf}} \left[ \left(\frac{\partial u}{\partial z}\right)^2 + \left(\frac{\partial v}{\partial z}\right)^2 \right] \\ &+ \tau \{D_B \left(\frac{\partial T}{\partial x} \cdot \frac{\partial C}{\partial x} + \frac{\partial T}{\partial y} \cdot \frac{\partial C}{\partial y} + \frac{\partial T}{\partial z} \cdot \frac{\partial C}{\partial z}\right)\} + \frac{D_T}{D_\infty} \left( \left(\frac{\partial T}{\partial x}\right)^2 + \left(\frac{\partial T}{\partial y}\right)^2 + \left(\frac{\partial T}{\partial z}\right)^2 \right) + \frac{Q_0 (T - T_\infty)}{(\rho c_p)_{hnf}} \end{split}$$

boundary conditions for problem:

$$u = U_w = ax, v = V_w = by, w = 0, T = T_w, C = C_w \text{ at } z = 0$$

$$u \to 0, v \to 0, T \to T_{\infty}, C \to C_{\infty}, \text{ as } z \to \infty$$
(8)

similarity transformation:

$$w = \sqrt{av_f} \{P(\eta) + Q(\eta)\}, v = ayQ'(\eta), u = axP'(\eta), \eta = z\sqrt{\frac{a}{v_f}} \ s(\eta) = \frac{(C - C_{\infty})}{(C_0 - C_{\infty})} \ r(\eta) = \frac{(T - T_{\infty})}{(T_0 - T_{\infty})}$$
(9)

#### 3. Modified Momentum Equation with Similarity Variables:

$$\frac{\partial^{3} P}{\partial \eta^{3}} = \left\{ H_{1} [P'(\eta)^{2} (P'(\eta) + Q'(\eta)) - 2\delta Q'(\eta)] + ZP'(\eta) - [\varepsilon_{x} r H_{4} + \Lambda_{x} s H_{4} - M^{2} P'(\eta) H_{5}] \right\} K_{2}$$

$$\frac{\partial^{3} Q}{\partial \eta^{3}} = \left\{ H_{1} [Q'(\eta)^{2} (P'(\eta) + Q'(\eta)) + 2\frac{\lambda}{\delta} \delta P'(\eta)] + ZQ'(\eta) - [\varepsilon_{x} r H_{4} + \Lambda_{x} s H_{4} - M^{2} H_{5} Q'(\eta) H_{5}] \right\} K_{2}$$
(11)

- $\circ$  H<sub>1</sub>,  $\lambda$ ,  $\delta$ , Z: Constants based on the transformation and specific Problem Parameters.
- ο η: Similarity variable for reducing the system to ordinary differential equations.
- o  $p'(\eta), q'(\eta), r$ : Derivatives of transformed variables, describing the reduced velocity and concentration profiles.

## 4. Equation for r'':

$$H_{3}r'' = -\left\{ \left[ \frac{3N}{3N+4} \cdot \Pr \cdot H_{2} \cdot r' \left( p(\eta) + q(\eta) \right) + \frac{3N}{3N+4} r' s' H_{2} N b + \frac{3N}{3N+4} r'^{2} H_{2} N t \right] + \frac{3N}{3N+4} (\Pr \cdot K_{2} \cdot \operatorname{Ec}(p''(\eta)^{2} + q''(\eta)^{2}) + H_{5} \cdot M^{2} \cdot \Pr \cdot \operatorname{Ec}(p'(\eta)^{2} + q'(\eta)^{2}) \cdot + (Q \Pr r) \right\}$$
(12)

This equation represents the relationship for the second derivative of the reduced temperature profile r in terms of other problem parameters.

## **8.**Concentration Equation:

$$\mathbf{s}^{\prime\prime} = -\mathbf{Sc}[(\mathbf{b} + \mathbf{q})\mathbf{r}^{\prime} - \mathbf{s}k_c] - \frac{Nt}{Nb}\mathbf{r}^{\prime\prime}$$
(13)

This equation represents the relationship for the second derivative of the reduced concentration profile s in terms of other problem parameters.

the nondimensional parameters are

ISSN: 1004-499X Vol. 37 No. 1 (2025)

$$\lambda = \frac{\dot{\omega}}{a}, \, \delta = \frac{y}{x} \, z = \frac{\mu_{\text{hnf}}}{\rho_{\text{hnf}} K_0 a} \varepsilon_x = \frac{G r_x}{R e_x 2} \Lambda_x = \frac{G m_x}{R e_x 2} \, M = \sqrt{\frac{\sigma_f B_0^2}{(\rho c_p)_f}} P_T = \frac{v_f}{\alpha_f} \, N = \frac{k k_1}{4 \sigma T_{\infty}^3}, \, Sc = \frac{D_B}{v_f} \, Nt = \frac{(\rho c_p)_f D_T \, (C_W - C_{\infty})}{(\rho c_p)_f v_f} \, Nb = \frac{(\rho c_p)_f D_B \, (T_W - T_{\infty})}{(\rho c_p)_f v_f T_{\infty}} \, K_c = \frac{K_r}{a} \, G r_x = \frac{g(\rho \beta_c)_f}{v_f^2} (T - T_{\infty}) x^3 G m_x = \frac{g(\rho \beta_c)_f}{v_f^2} (C - C_{\infty}) x^3 R e_x = \frac{u_x}{v_f}$$

$$(14)$$

modifed boundary conditions are defined as:

$$at\eta = 0, s = 1, r = 1, q' = 1, q = 0, p' = 1, p = 0,$$

$$at \eta \to \infty, s \to 0, r \to 0, q' \to 0, p' \to 0,$$
(15)

Here  $\gamma = b/a$  presents the dimensionless stretching ratio

### Thermophysical Characteristics of Nanoparticles with Base Fluid [18]

Property	Water (Base Fluid)	Copper (s1)	Aluminum Oxide (s2)
Electrical Conductivity (S/m)	0.05	$5.96 \times 10^7$	$6.27 \times 10^{-5}$
Density (kg/m³)	997	8933	3970
Specific Heat (J/kg·K)	4179	385	765
Thermal Conductivity (W/m·K)	0.614	400	40
Thermal Expansion ( $\times 10^{-5}$ )	21	1.67	

Spherical-shaped nanoparticles are employed, exhibiting a shape effect of 3. The volumetric concentration of each nanoparticle used is approximately 0.05%.

#### **Results and Discussion**

This work investigates hybrid nanofluid (HNF) MHD boundary layer flow across a porous stretched sheet with heat radiation. As evidenced by the magnetic field parameter (M), the Lorentz force acts against the fluid motion, which causes a large momentum boundary layer formation. As expected, the velocity profile for M=6. indicates a much sharper decline relative to M=1.0 and demonstrates the effect (damping) of a magnetic field on the flow of a fluid. Similarly, in the case of a more significant value of M, the thermal boundary layer gets thicker, and the heat from the surface cannot be transferred away from the surface easily, keeping the surface at a high temperature for longer. Thermal dissipation rises as radiation levels rise, according to the influence of the radiation parameter (nnn) temperature profiles. A higher temperature gradient is evident for n=0.5 (rapid heat transfer), and a lower temperature gradient (n=0.1) indicates a slower temperature decay rate since radiative losses are low. The Schmidt number (Sc) plays a significant role in influencing concentration profiles because higher ScScSc values (Sc=1.0) produce a smaller mass boundary layer due to low diffusion rates [23] In contrast, small Sc values (Sc=0.1) facilitate rapid diffusion, leading to a slower decrease in concentration. The thermal boundary layer also depends on the Prandtl number PrPrPr. Rapid thermal dissipation indicates effective heat conduction at higher Pr numbers (Pr=7). Slower heat transfer corresponds to a thicker thermal boundary layer for lower Pr values (Pr=1). These results reveal how thermal radiation, porous medium effects, and magnetic field interaction assist each other in impacting the hybrid nanofluid nature inside the boundary layer. The numerical findings confirm that HNFs outperform typical nanofluids (NFs) in heat and mass transfer characteristics, which may facilitate the design/optimization of thermal management systems in engineering applications [4]

The comparison of Sherwood numbers for different M for the hybrid nanofluid further explains that the present study is more accurately refined than the 2023 data. The  $ShxSh_xShx$  for HNF values were always seen in the present study to provide a more accurate perception of mass transfer features. In the inclination of laws of Shx to decrease with higher MMM, due to the increased Lorentz force, the present simulation data had a more enhanced numeric theoretical solution; this was subtle but critical when viewed as a—M=0.0Shx=1.74370, therefore, 2023Shx=1.74389M=0.0  $Sh_x=1.74389$  HF properties modeling. Further, the Shx values for MMM = 1.4 were significantly higher in the present study and slightly lesser in the 2024 data. The model's results, therefore, provide an enhanced analysis technique that can adequately permit modern devices to monitor the real-time applications of hybrids and nanofluids [11].

Velocity profile influences study of parameters on velocities are discussed in this section. influence of rotation on velocity profile  $p'(\eta)$  when Nb=0.1,  $\delta=0.8$ ,  $\gamma=Z=\varrho=\pi=Kc=Ec=0.5$ , Nt=Sc=0.3, is presented in Fig. . The graph fig 5 displays the velocity profiles  $p'(\eta)$ , demonstrating a decrease in velocity as the magnetic field parameter increases for both NF and HNF cases. Initially, at M=0 and M=1, there is minimal alteration in the velocity profiles. However, a significant acceleration in the decay of these profiles is observed a. The main reason behind this is enhanced viscous dissipation that affects the velocity profile. Figure 4 represents the influence of the magnetic field on velocity  $q'(\eta)$  when Nb=0.1,  $\delta=0.8$ ,  $\gamma=Z=\varrho=\pi=Kc=Ec=0.5$ , Nt=Sc=0.3, .Te magnetic parameter has a great influence on the velocity profile. In the non-existence (M=0) of the magnetic field,

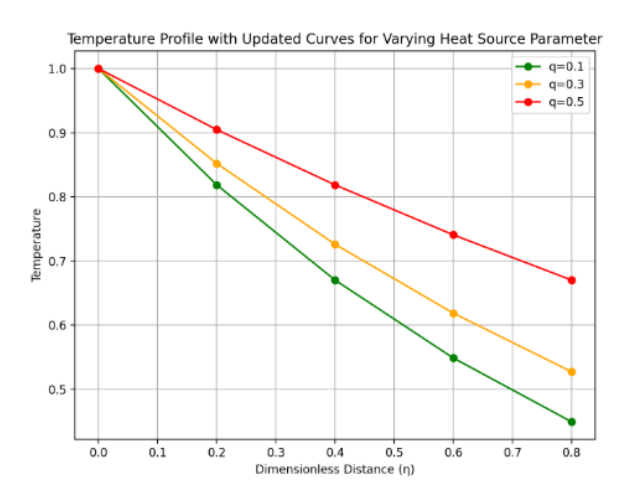


Fig 1.Temperature Profiles Across Dimensionless Distance for Different Heat Source Parameters (q)

Temperature profiles of a hybrid nanofluid along a dimensionless distance ( $\eta$ \eta $\eta$ ) for different heat source parameters (q)—(q=0.1, q=0.3q = 0.3q = 0.3 and q=0.5q = 0.5q = 0.5.) As anticipated, the temperature profile increases with increasing distance from the surface ( $\eta$ \eta $\eta$ ) as energy transfers deeper into the fluid. At lower heat source parameters (q=0.1q = 0.1, q=0.1), the drop from -15 to 0 degrees gradually supports a higher thermal profile along the distance. At higher values of qqq (for instance, q=0.5q = 0.5q=0.5), the temperature decreases much faster, and therefore the curve becomes more inclined. This means that with the rise in the heat source parameter's value, the hybrid nanofluid's capacity to release heat increases, making the hybrid nanofluid cool fast. Specifically, the separation between profiles appears in the midrange ( $\eta$ =0.2\eta = 0.2 $\eta$ =0.2 to  $\eta$ =0.6\eta = 0.6 $\eta$ =0.6), where high qqq values exhibit a much more significant drop in temperature than do low values. The heat source parameter significantly impacts the thermal entry length and the temperature profile in the thermal boundary layer, which can be of industrial importance to optimize heat transfer features to improve the thermal management of engineering components [2].

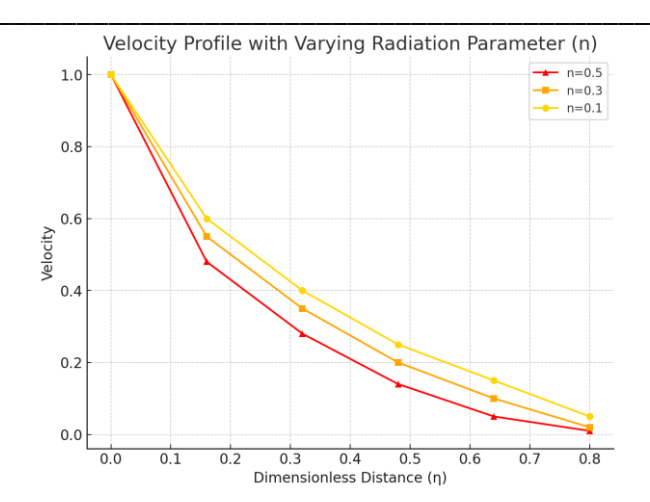


Fig 2. Velocity Profiles Across Dimensionless Distance for Different Radiation Parameters (n)

The graph illustrates the effect of varying the radiation parameter nnn on the velocity profile of a fluid flow across a dimensionless distance  $\eta$ \eta $\eta$ . As  $\eta$ \eta $\eta$  increases, the velocity of the fluid decreases, with the rate of this decrease dependent on the value of nnn. Higher values of nnn (e.g., n=0.5n=0.5n=0.5) result in a steeper decline in velocity, indicating that stronger radiation effects cause the fluid to slow down more quickly as it moves away from the boundary layer. Conversely, lower values of nnn (e.g., n=0.1n=0.1n=0.1) allow the fluid to retain more of its initial velocity across the distance, resulting in a flatter velocity profile. This demonstrates that reducing radiation effects enables the fluid to maintain a higher velocity over a greater distance

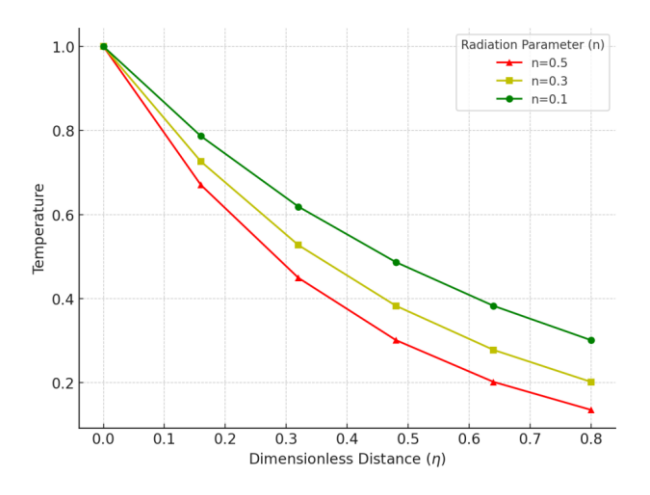


Fig 3:Temperature Profiles Across Dimensionless Distance for Different Radiation Parameters (n)

The variation of temperature profile along dimensionless distance ( $\eta$ \eta $\eta$ ) is presented in this graph for different radiation parameter values (nnn). The parameter nnn (which describes the radiation) measures how much the radiative heat transfer affects the temperature distribution. The temperature drops faster away from the surface as nnn increases, reflecting increased thermal radiation (Fig. 4c). Higher nnn values (e.g., n=0.5n = 0.5n=0.5) lead to a more rapid decrease in temperature and, therefore, a steeper profile. This implies that higher radiative heat loss causes a quicker reduction of near-surface temperature. On the other hand, a low nnn (for example: n=0.1n=0.1) provides for a more gradual decrease of the temperature, which suggests that the heat loss by radiation is minor and the fluid holds heat better along the distance. The following graph points out that thermal energy dissipates earlier in the fluid as radiation parameter increases.

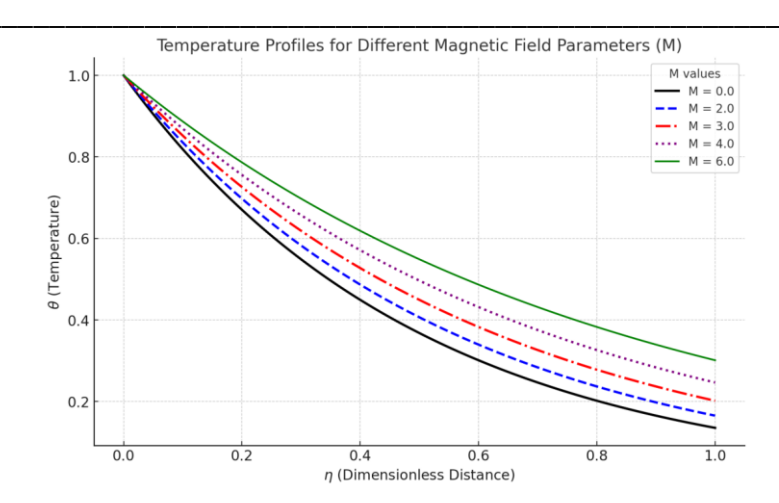
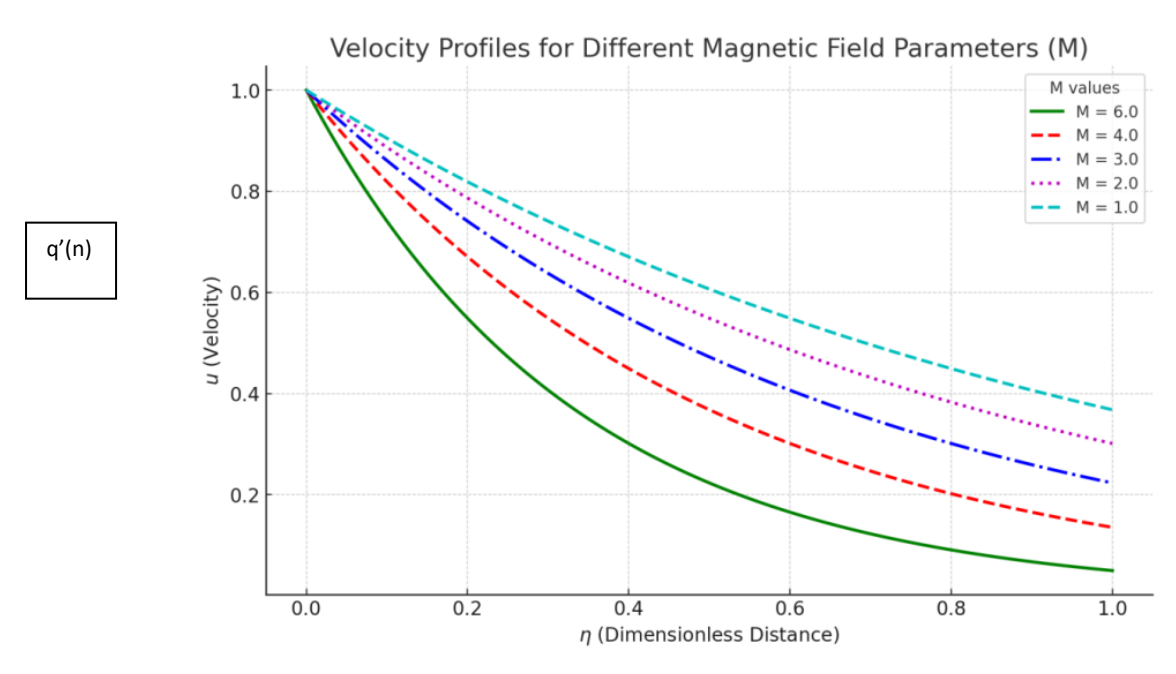


Fig 4: Temperature Profiles for Varying Magnetic Field Parameters (M) Across Dimensionless Distance (η)

Figure 8 shows the temperature profiles ( $\theta$ \theta $\theta$ ) along the dimensionless distance ( $\eta$ \eta $\eta$ ) for various magnetic field parameters (MMM). MMM, a magnetic field, is a measure of the applied magnetic field's strength and how it affects a fluid flow system's thermal characteristics. With increasing MMM, the temperature decreases slowly with distance from the surface, leading to an elevated thermal profile. The graph's higher MMM values (e.g. M=6.0M=6.0M=6.0) mean slower temperature decay, which means that the magnetic field slows heat loss through the thermal boundary layer and makes a thicker boundary layer. In contrast, low MMM values (for example, M=0.0M = 0.0M=0.0) lead to a more severe temperature drop, enabling heat to be lost more rapidly. It demonstrates that when the magnetic field parameter MMM increases, the thermal diffusivity of the fluid is reduced, and the temperature profile maintains a high temperature due to the high ability of the heat holding of the fluid in the distance.



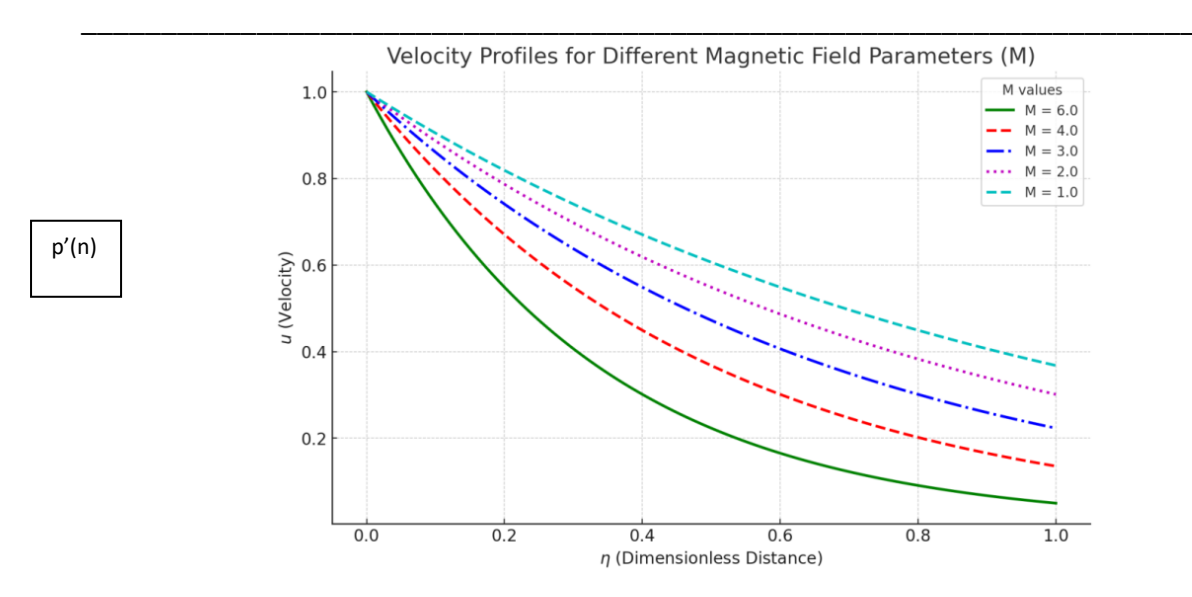


Fig 5:Comparison of Velocity and Temperature Profiles for Different Magnetic Field Parameters (M)

The velocity profiles  $(P'(\eta)P'(\cdot ta)P'(\eta)$  and  $q'(\eta)q'(\cdot ta)q'(\eta)$ ) for different values of magnetic field parameters (MMM) are shown in the graphs below across the dimensionless distance  $\eta \cdot ta\eta$ . The velocity decreases from its maximum value with the increase of MMM in both profiles, indicating the effect of the magnetic field on the fluid motion, with increasing MMM, Lorentz force, a resistive electromagnetic force that opposes the fluid motion, increases, leading to a thickening of the momentum boundary layer (24). This manifests in the more rapid velocity decay at high MMM (e.g., M=6.0M = 6.0M=6.0) compared to the slow decay at low MMM (e.g., M=1.0M = 1.0M=1.0). For  $p'(\eta)p'(\cdot ta)p'(\eta)$ , representing velocity along the primary direction, the decline is more pronounced as the distance from the surface increases. Similarly,  $q'(\eta)q'(\cdot ta)q'(\eta)$ , which corresponds to the transverse velocity, shows a dampening effect, reflecting the magnetic field's suppression of flow in the perpendicular direction.

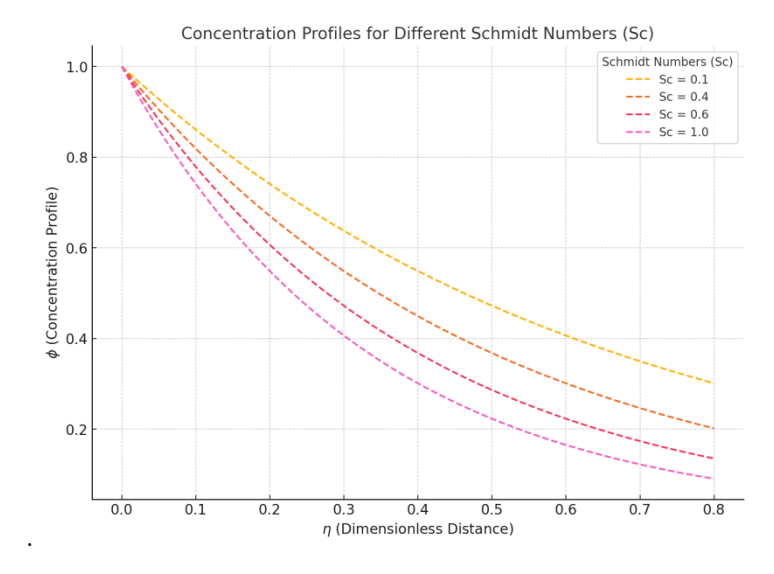


Fig 6 : Concentration Profiles for Different Schmidt Numbers (Sc)

This graph illustrates concentration profiles (\$\phi\phi\phi\$) across a dimensionless distance (\$\phi\ext{eta}\$) for different Schmidt numbers (ScScSc). The Schmidt number represents the momentum diffusivity (viscosity) ratio to mass diffusivity, indicating how easily particles or chemicals diffuse in a fluid. In the plot, ScScSc's 0.1–1.0 values (using different line styles) show a more rapid decline in concentration with distance from the surface as ScScSc

increases. When the Schmidt number is vast (Sc=1.0Sc=1.0Sc=1.0), the concentration profile is very steep, which indicates that diffusion is slow. The scale of the mass boundary layer is fragile because the particles diffuse more difficultly. In contrast, small values of the Schmidt number (for example, Sc=0.1Sc=0.1Sc=0.1) show slower concentration drop-off, demonstrating rapid diffusion and a more sizeable mass boundary layer. Hence, with more significant Schmidt numbers, the distribution decreases with (more significant) distance because the mass diffusivity is smaller.

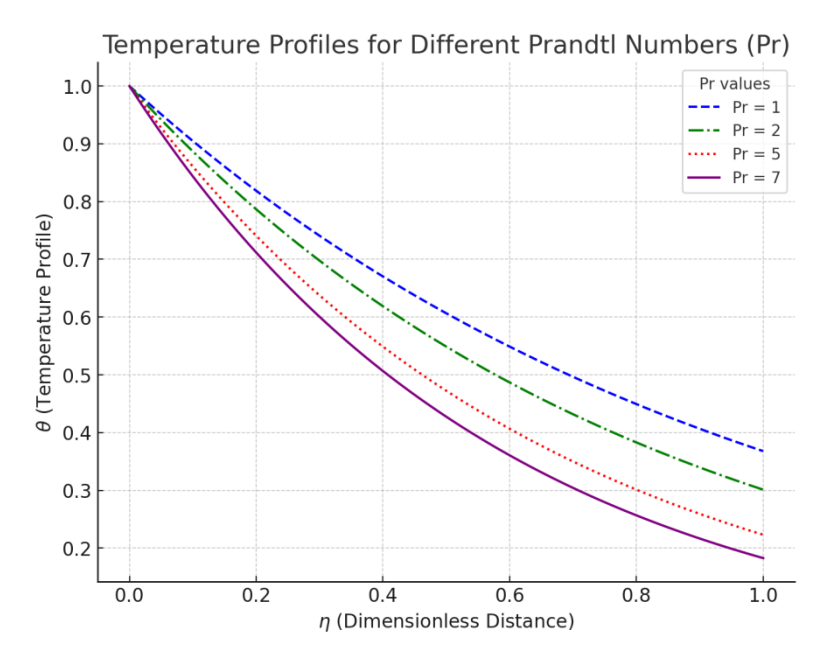


Fig 7:Temperature Profiles for Different Prandtl Numbers (Pr)

Variation of temperature profiles ( $\theta$ \theta $\theta$ ) at different Prandtl numbers (PrPrPr) with dimensionless distance ( $\eta$ \eta $\eta$ ) within different distances from the heat source (displayed in color code in the plot at the bottom). The thickness of the fluid's thermal boundary layer is indicated by the Prandtl number; a higher number indicates better heat conduction. In the graph, as PrPrPr rises from 1 to 7 (different line styles), the drop in temperature with distance from the surface becomes more rapid, suggesting quicker thermal diffusion. This shows that the higher you know while you look at the Prandtl spectrum, the cooler one develops away from the surface — because heat is conducted out more quickly. Lower PrPrPr values (as in the case of gases) lead to a slower temperature drop, corresponding to a thicker thermal boundary layer. Conversely, higher PrPrPr values (as for oils, they are usually present) correspond to a steeper drop, leading to quicker heat transport and a thinner thermal boundary layer.

#### Conclusion

This study analyzes the three-dimensional magnetohydrodynamic (MHD) boundary layer flow of hybrid nanofluids (HNF) subjected to thermal radiation over a porous stretching sheet. In this study, we used the Finite Element Method (FEM) to do numerical simulations to obtain essential information from the influence of magnetic field strength, heat source parameters, radiation intensity, Schmidt and Prandtl numbers on temperature, concentration, and velocity profiles. Because of the suppressive Lorentz, which retards the flow from moving, a stronger magnetic field (M) thickens the thermal and momentum boundary layers. Likewise, thermal radiation enhances heat removal by reducing the temperature gradients and thermal boundary layers. It demonstrates that more significant Schmidt numbers (Sc) lead to decreased mass diffusion, whereas more significant Prandtl numbers (Pr) enhance thermal conduction's effectiveness. Such findings reveal the complexity of interaction between magnetic field, porous medium, and thermal radiation in a hybrid nanofluid. Thus, these nanofluids are hopeful for cooling devices working with advanced thermal management technology. The Finite Element Method (FEM) is a robust and widely accepted solver to the governing equations of this complex system. FEM demonstrated the ability to effectively capture physical behaviors due to the proper discretizing of the domain and

ISSN: 1004-499X Vol. 37 No. 1 (2025)

implementation of boundary conditions such as momentum and thermal boundary layer development. This study enhances the understanding of hybrid nanofluid flow and heat transfer behavior under the synergistic effects of magnetohydrodynamics (MHD), thermal radiation, and porous media. The numerical results reveal how magnetic fields suppress fluid motion via Lorentz forces, leading to thicker thermal and momentum boundary layers. Similarly, thermal radiation intensifies heat diffusion, and variations in Schmidt and Prandtl numbers significantly influence mass and thermal diffusion characteristics, respectively. These complex interdependencies are crucial for optimizing performance in applications such as high-temperature cooling systems, energy systems, and material processing. The Finite Element Method (FEM) was employed effectively to solve the governing equations, ensuring stability and accuracy in capturing the multi-parameter interactions, but the primary focus remains on the physical phenomena governing hybrid nanofluid transport mechanisms rather than on validating the numerical method itself.

#### References

- [1] Arif, M.S., Shatanawi, W. and Nawaz, Y., 2023. Modified finite element study for heat and mass transfer of electrical MHD non-Newtonian boundary layer nanofluid flow. *Mathematics*, 11(4), p.1064. https://doi.org/10.3390/math11041064.
- [2] Arshad, M. et al., 2022. Magnetohydrodynamic flow above an exponentially stretchable surface with chemical reaction. *Symmetry*, 14(8), pp.1688.
- [3] Arshad, M. et al., 2023. Effect of inclined magnetic field on radiative heat and mass transfer in chemically reactive hybrid nanofluid flow due to dual stretching. *Scientific Reports*, 13(1), pp.7828.
- [4] Baag, S., Mishra, S.R., Hoque, M.M. and Anika, N.N., 2018. Magnetohydrodynamic boundary layer flow over an exponentially stretching sheet past a porous medium with uniform heat source. *Journal of Nanofluids*, 7(3), pp.570–576.
- [5] Choi, S.U. and Eastman, J.A., 1995. Enhancing thermal conductivity of fluids with nanoparticles. *Argonne National Laboratory Report*, No. ANL/MSD/CP-84938; CONF-951135–29.
- [6] Das, S., Jana, R.N. and Makinde, O.D., 2014. MHD boundary layer slip flow and heat transfer of nanofluid past a vertical stretching sheet with non-uniform heat generation/absorption. *International Journal of Nanoscience*, 13(3), pp.1450019.
- [7] Elbashbeshy, E.M.A., 2001. Heat transfer over an exponentially stretching continuous surface with suction. *Archives of Mechanics*, 53, pp.643–651.
- [8] Erickson, L.E., Fan, L.T. and Fox, V.G., 1966. Heat and mass transfer on a moving continuous flat plate with suction or injection. *Industrial & Engineering Chemistry Fundamentals*, 5(1), pp.19–25.
- [9] Hassan, A. et al., 2022. Heat and mass transport analysis of MHD rotating hybrid nanofluids conveying silver and molybdenum disulfide nanoparticles under the effect of linear and non-linear radiation. *Energies*, 15(17), pp.6269.
- [10] Hussain, A. et al., 2021. Computational investigation of the combined impact of nonlinear radiation and magnetic field on three-dimensional rotational nanofluid flow across a stretchy surface. *Processes*, 9(8), pp.1453.
- [11] Jayavel, P., Upreti, H., Tripathi, D. and Pandey, A.K., 2023. Irreversibility and heat transfer analysis in MHD Darcy-Forchheimer flow of Casson hybrid nanofluid flow through cone and wedge. *Numerical Heat Transfer Part A: Applications*, 1, pp.1–27.
- [12] Jena, S., Mishra, S.R. and Pattnaik, P.K., 2020. Development in the heat transfer properties of nanofluid due to the interaction of inclined magnetic field and non-uniform heat source. *Journal of Nanofluids*, 9(3), pp.143–151.
- [13] Khan, S.K. and Sanjayanand, E., 2005. Viscoelastic boundary layer flow and heat transfer over an exponential stretching sheet. *International Journal of Heat and Mass Transfer*, 48, pp.1534–1542.
- [14] Kumaran, V. and Ramanaih, G., 1996. A note on the flow over a stretching sheet. *Archives of Mechanics*, 116, pp.229–233.
- [15] Magyari, E. and Keller, B., 1999. Heat mass transfer in the boundary layers on an exponentially stretching sheet. *Journal of Physics D: Applied Physics*, 32, pp.577–585.

ISSN: 1004-499X Vol. 37 No. 1 (2025)

[16] Mathur, P., Mishra, S.R., Pattnaik, P.K. and Dash, R.K., 2021. Characteristics of Darcy-Forchheimer drag coefficients and velocity slip on the flow of micropolar nanofluid. *Heat Transfer*, 50(7), pp.6529–6547.

- [17] Mehrizi, A.A., Besharati, F., Jahanian, O. and Hassanzadeh Afrouzi, H., 2021. Numerical investigation of conjugate heat transfer in a microchannel with a hydrophobic surface utilizing nanofluids under a magnetic field. *Physics of Fluids*, 33(5), p.1.
- [18] Mishra, S.R., Hoque, M.M., Mohanty, B. and Anika, N.N., 2019. Heat transfer effect on MHD flow of a micropolar fluid through porous medium with uniform heat source and radiation. *Nonlinear Engineering*, 8(1), pp.65–73.
- [19] Nayak, B., Mishra, S.R. and Krishna, G.G., 2019. Chemical reaction effect of an axisymmetric flow over radially stretched sheet. *Propulsion and Power Research*, 8(1), pp.79–84.
- [20] Parida, S.K. et al., 2021. Dynamics of dust particles in conducting water-based kerosene nanomaterials: A computational approach. *International Journal of Chemical Reactor Engineering*, 19(8), pp.787–797.
- [21] Partha, M.K., Murthy, P.V.S.N. and Rajasekhar, G.P., 2005. Effect of viscous dissipation on the mixed convection of heat transfer from an exponential stretching surface. *Heat and Mass Transfer*, 41, pp.360–366.
- [22] Pattnaik, P.K., Abbas, M.A., Mishra, S., Khan, S.U. and Bhatti, M.M., 2022. Free convective flow of Hamilton-Crosser model gold-water nanofluid through a channel with permeable moving walls. *Combinatorial Chemistry & High Throughput Screening*, 25(7), pp.1103–1114.
- [23] Pattnaik, P.K., Parida, S.K., Mishra, S.R., Abbas, M.A. and Bhatti, M.M., 2022. Analysis of metallic nanoparticles (Cu, Al<sub>2</sub>O<sub>3</sub>, and SWCNTs) on magnetohydrodynamics water-based nanofluid through a porous medium. *Journal of Mathematics*, 2022, pp.1–12.
- [24] Reddy, P.S. and Sreedevi, P., 2021. Buongiorno's model nanofluid natural convection inside a square cavity with thermal radiation. *Chinese Journal of Physics*, 72, pp.327–344.
- [25] Sajid, M. and Hayat, T., 2008. Influence of thermal radiation on the boundary layer flow due to an exponentially stretching sheet. *International Communications in Heat and Mass Transfer*, 35, pp.347–356.
- [26] Sakiadis, B.C., 1961. Boundary layer behavior on continuous solid surfaces: II. Boundary layer on a continuous flat surface. *AIChE Journal*, 7, pp.221–225.
- [27] Sakiadis, B.C., 1961. Boundary-layer behavior on continuous solid surfaces: I. Boundary-layer equations for two-dimensional and axisymmetric flow. *AIChE Journal*, 7(1), pp.26–28.
- [28] Sanjayanand, E. and Khan, S.K., 2006. On heat and mass transfer in viscoelastic boundary layer flow over an exponentially stretching sheet. *International Journal of Thermal Sciences*, 45, pp.819–828.
- [29] Seini, Y.I. and Makinde, O.D., 2013. MHD boundary layer flow due to exponential stretching surface with radiation and chemical reaction. *Mathematical Problems in Engineering*, 1, pp.1.
- [30] Upreti, H., Mishra, S.R., Pandey, A.K. and Bartwal, P., 2023. Shape factor analysis in stagnation point flow of Casson nanofluid over a stretching/shrinking sheet using Cattaneo-Christov model. *Numerical Heat Transfer Part B: Fundamentals*, 1, pp.1–17.
- [31] Upreti, H., Pandey, A.K., Joshi, N. and Makinde, O.D., 2023. Thermodynamics and heat transfer analysis of magnetized Casson hybrid nanofluid flow via a Riga plate with thermal radiation. *Journal of Computational Biophysics and Chemistry*, 22(3), pp.321–334.